Microscopic origin and energy levels of the states produced in *a*-Si:H by phosphorus doping

J. Kočka and J. Stuchlík
Institute of Physics, Academy of Sciences of Czech Republic, Cukrovarnická 10, 162 00 Prague 6, Czech Republic

M. Stutzmann
Max-Planck-Institut für Festkörperforschung, Heisenbergstrasse 1, D-7000 Stuttgart 80, Germany

L. Chen and J. Tauc
Division of Engineering and Department of Physics, Brown University, Providence, Rhode Island 02912
(Received 21 August 1992)

In order to clarify the origin of the phosphorus-related hyperfine-electron-spin-resonance (ESR) signal we study the properties of differently P-doped amorphous hydrogenated silicon (*a*-Si:H) prepared at low substrate temperature ($T_s = 50\,^{\circ}\mathrm{C}$) and the changes induced by subsequent annealing at temperatures up to $T_A = 250\,^{\circ}\mathrm{C}$. In addition to the standard ESR and electrical conductivity we use light-induced ESR, subgap absorption, and photomodulation spectroscopy to characterize the samples. We have found that part of the controversy concerning the origin of the phosphorus hyperfine (hf) signal is related to the fact that the usual assumptions, namely that the sample is homogeneous, the conduction-band edge energy E_C is fixed, and only the Fermi level E_f moves are not satisfied. When the substrate temperature decreases from 250 to 50 °C the hydrogen content and the optical gap of P-doped *a*-Si:H increases and the anti-Meyer-Neldel behavior indicates the shift of the transport path (E_C). Although the total density of deep defects changes only slightly by annealing, their character changes substantially. To explain the details of the ESR results heterogeneity given by long-range potential fluctuations must be introduced.

I. INTRODUCTION

The work by Spear and LeComber,[1] which demonstrated that hydrogenated amorphous silicon (*a*-Si:H) can be doped, stimulated development of the study of amorphous semiconductors. Although the basic principle of doping of amorphous semiconductors (the so-called modified 8-*N* rule), introduced by Street,[2] is generally accepted, a number of doping-related problems remain unresolved.

Electron-spin-resonance (ESR) measurements significantly contributed to the understanding of the microscopic nature of the defects in *a*-Si:H. Three basic ESR signals[3] have been observed in *a*-Si:H with the ESR *g* values of $g \approx 2.0055$, 2.0044, and 2.013, respectively, which have been attributed to the electron of a singly occupied silicon dangling bond (db), electrons trapped in the conduction band (cb), and holes in the valence-band (vb) tail, respectively. Later, another ESR hyperfine line (hf) was observed in P-doped *a*-Si:H,[4,5] and attributed to the shallow fourfold-coordinated phosphorus donor (P_4^0) state[4] or to the deep phosphorus-related states (twofold-coordinated phosphorus—P_2^0 or "weak" P_4^0).[5,6]

The basic argument against the original assignment (P_4^0) of the p-hf signal has been that an almost identical hf signal as that in the device-quality[4,5] *a*-Si:H:P (substrate temperature $T_s \approx 250\,^{\circ}\mathrm{C}$), is also observed[7] in *a*-Si:H:P prepared at $T_s = 50\,^{\circ}\mathrm{C}$. For this low-$T_s$ sample the electrical conductivity activation energy $E_a \approx 0.59$ eV has been found and used as an argument that the shallow P_4^0 state should be depopulated in this case. With the exception of Ref. 7, all other results have been obtained on as-prepared[4,5] or electron-irradiated[8] device-quality *a*-Si:H:P samples ($T_s = 250\,^{\circ}\mathrm{C}$).

In order to clarify the existing controversies, the aim of this paper is to present additional experimental results on differently doped *a*-Si:H:P samples prepared at $T_s = 50\,^{\circ}\mathrm{C}$, with the information gained by studying annealing and by complementary characterization of these samples. In addition to the results of transport and ESR measurements, we will present light-induced ESR results (LESR) and also the steady-state photomodulation and subgap absorption results, which give important information about the energy positions and density of the main defects. In a certain sense, the annealing of low-T_s samples is the opposite process to the electron irradiation[8] of device-quality *a*-Si:H:P. But there is a substantial difference in one point—the low-T_s samples contain much more hydrogen[9] (up to ≈ 35 at.%).

This paper is organized as follows. In Sec. II we present the experimental details. Section III—experimental results—is divided into four parts dealing with the electrical conductivity, band-gap and subgap absorption, photomodulation and finally the ESR results, each with a short discussion. Section IV contains a general discussion of the experimental results and the conclusions.

II. EXPERIMENT

The *a*-Si:H:P samples were prepared at the substrate temperature $T_s = 50\,^{\circ}\mathrm{C}$ by rf glow-discharge decomposi-

tion of the mixture of pure silane (SiH_4) with 0.1% or 1% admixture of phosphine (PH_3). During the preparation we used a SiH_4 flow rate of 30 sccm and maintained the pressure at 0.2 mbar. The sample thickness was in the range 2–5 μm.

The measurement of the electrical conductivity was done for a-Si:H deposited on Corning 7059 glass substrate in a coplanar contact arrangement with a 2-mm distance of the coplanar contacts and typically 40 V applied voltage.

The same samples were used for the measurement of the photoconductivity by the constant-photocurrent method (CPM).[10] In addition, the 2-mm gap distance also allowed us to perform the photothermal-deflection-spectroscopy (PDS) (Ref. 11) measurement on the same samples in the area between the metal contacts. Annealing of these samples was done under He atmosphere typically up to 150 °C, in some cases up to 250 °C.

Spin-resonance measurements were performed at 300 K (ESR) and 100 K (ESR and LESR) using a Bruker 300 X-band spectrometer with computerized averaging and background subtraction. Magnetic-field modulation with a frequency of 100 kHz was used and microwave power levels were kept sufficiently low (100 μW at 100 K) to avoid saturation effects. Samples were deposited on thin Al foils and the Al substrate was dissolved in dilute HCl. The obtained a-Si:H flakes were filtered, washed, and dried, and then collected in annealed spin-free quartz tubes. Typically 10–20 mg of a-Si:H were used for the ESR measurements. Annealing of the samples was performed in ambient atmosphere inside the tubes. For LESR measurements the samples were illuminated inside the ESR microwave cavity with white light from a tungsten lamp or with homogeneously absorbed monochromatic light from a Ti-sapphire laser, using an optical fiber system. Spin densities were calibrated using the phosphorus hyperfine lines in crystalline silicon with a known carrier density as the primary standard.

For the steady-state photomodulation (PM) spectroscopy,[12] an Ar^+ laser (photon energy 2.4 eV, intensity 100 mW/cm^2) was used as the steady-state pump. The probe photon energy was scanned in the range 0.06–2 eV. Between 0.06 and 0.30 eV we used a Fourier-transform infrared spectrometer (Bomen model DA-3.01) and the PM spectra were determined as the difference between the spectra measured with the pump on and off. In the range 0.25–2 eV we used a grating monochromator. The pump light was chopped at 75 Hz and the photoinduced change of the transmission (ΔT) was measured. The system spectral response function was accounted for by taking the ratio $\Delta T/T$.

It has been shown[12] that in a-Si:H the relative changes in reflectivity $\Delta R/R$ in our spectral range are small compared to $\Delta T/T$. In this case, $\Delta T/T=-\Delta\alpha/\alpha_p$, where $\Delta\alpha$ is the photoinduced change in the absorption coefficient and α_p is the absorption coefficient of the pump light. The spectral resolution was better than 50 meV (grating monochromator) and 5 meV (Fourier-transform spectrometer). The value $\Delta T/T$ was in the range 10^{-5}–10^{-3}. For PM studies, the a-Si:H films were deposited on sapphire or crystalline Si substrates.

III. EXPERIMENTAL RESULTS

A. Electrical conductivity

In Fig. 1 the temperature (T) dependences of the electrical conductivity (σ) of as-prepared ($T_s=50$ °C) and step-by-step annealed 0.1% PH_3-doped a-Si:H:P samples are shown.

The conductivity was measured during a slow increase of the temperature. When the specific annealing temperature was reached, the sample stayed at this temperature for 15 min and then was slowly cooled down, and the conductivity was measured again.

From the slope of logσ versus $1000/T$ we can deduce the measured activation energy (E_a) and the prefactor (σ_0) defined by the equation

$$\sigma(T)=\sigma_0\exp(-E_a/kT) \tag{1}$$

where k is the Boltzmann constant, E_a is equal to the difference between the Fermi level (E_f) and the mobility edge (E_c) at $T=0$ K. To deduce E_c-E_f at room temperature (RT) from these data, we should know the temperature shift of E_c and E_f and this presents a rather complex problem. Very often $\sigma_0=200\ \Omega^{-1}\,\mathrm{cm}^{-1}$ is assumed (substantiated by theoretical reasons and some experimental results)[13] so that the difference (E_c-E_f) at room temperature can also be directly calculated from the value of the room-temperature conductivity (σ_{RT}). We label this value $E_{200}=E_c(\mathrm{RT})-E_f(\mathrm{RT})$.

In Fig. 2 results for σ_{RT} (measured at RT after annealing) and E_{200} are plotted as a function of annealing tem-

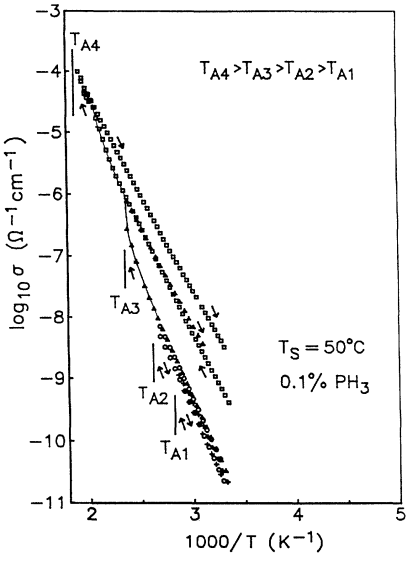

FIG. 1. Temperature dependence of electrical conductivity σ of 0.1% PH_3-doped a-Si:H:P, prepared at $T_s=50$ °C, subjected to step-by-step annealing. The sample was slowly heated to the preselected annealing temperature (T_A), stayed at this temperature for 15 min, and then was again cooled to RT. During the heating and cooling the conductivity was recorded. In the next step the heating to the higher T_A was performed.

TABLE I. *a*-Si:H:P transport data (*V* denotes virgin, *A* denotes annealed. See text).

PH_3/SiH_4 T_s	State	σ_0 (Ω^{-1} cm^{-1})	E_a (eV) meas.	E_{200} (eV) calc.
0.1% 50 °C	*V*	4	0.69	0.79
	A (150 °C)	70	0.66	0.69
1% 50 °C	*V*	0.6	0.49	0.63
	A (150 °C)	0.3	0.40	0.56
1% 250 °C	*V*	10	0.19	0.26
	A (150 °C)	14	0.19	0.24

perature (T_A). It is seen that there are no changes up to about $T_A = 80$ °C. The most dramatic changes (inflection point) occur at about 130 °C, which is near the equilibrium temperature for P-doped *a*-Si:H,[14] both probably controlled by H movement. The data for a 1% PH_3-doped $T_s = 50$ °C *a*-Si:H:P sample have a similar character.

In Table I we have summarized the basic transport data of $T_s = 50$ °C samples (0.1% and 1% PH_3 doped) and the same results for $T_s = 250$ °C, 1% PH_3-doped *a*-Si:H:P, which are shown for comparison.

In device-quality *a*-Si:H the prefactor σ_0 and E_a (changed, for example, by doping) are related by the so-called Meyer-Neldel rule,[13,15] which very roughly means that with increasing E_a also σ_0 increases. The Meyer-Neldel (MN) rule can be explained by the Fermi-level (E_f) statistical shift in a realistic model for the density of localized states.[16] Comment on the recent, more general explanation of the MN rule is in Sec. IV. The validity of the MN rule, together with the fact that the optical and the mobility gap[17] of a device-quality *a*-Si:H does not change with the *n*-type doping, substantiates the usual assumption that the electron mobility edge E_c does not move and the observed changes of E_a are related predominantly to the E_f shift.

From the comparison of $T_s = 250$ °C and 50 °C data for 1% PH_3-doped *a*-Si:H:P in Table I it is seen that the decrease of T_s from 250°–50 °C leads to *increase* of E_a but, contrary to the Meyer-Neldel rule, to a strong *decrease* of σ_0. The same "anti-Meyer-Neldel" tendency is seen also for the effect of the 150 °C annealing of 0.1% PH_3-doped $T_s = 50$ °C sample. This is a strong indication that the transport path (E_c) is moving and the procedure used in device-quality samples (fixed E_c and $\sigma_0 = 200\ \Omega^{-1}\,\mathrm{cm}^{-1}$), cannot be generally used.

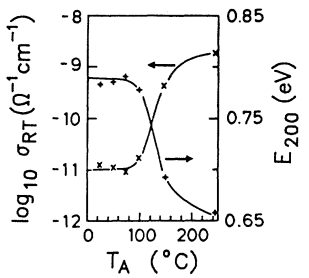

FIG. 2. Room-temperature electrical conductivity (σ_{RT}) and activation energy E_{200} deduced on the basis of Fig. 1 as a function of temperature (T_A) of 15-min annealing.

B. Band-gap and subgap absorption

To obtain information about the total number of deep defects we have used the same samples on which the electrical conductivity was measured for the CPM (Refs. 10 and 18) and PDS measurements.

In Fig. 3 we show the spectral dependence of absorbance of a 1% PH_3, $T_s = 50$ °C *a*-Si:H:P sample in the as-prepared (virgin) state and after 150 °C annealing. Additional 250 °C annealing led to a small (about 30%) additional decrease of the subgap shoulder.

The PDS and CPM curves at the high-energy side agree quite well. The origin of the small difference in the shape of the subgap shoulder between CPM and PDS is not clear at present. The density of defects estimated from the CPM data agrees very well with the ESR data (see below).

An interesting fact is that contrary to the low-T_s undoped *a*-Si:H in which annealing dramatically reduces the subgap absorption shoulder,[19] in our low-T_s 1% doped samples annealing decreases the shoulder only by a factor of 2. The same is true also for 0.1% PH_3-doped low-T_s *a*-Si:H:P samples.

While the mobility gap is not easy to measure, another important parameter, the optical gap (E_g), can be deduced from the transmission data by a standard procedure[20]—a plot of the spectral dependence of $(\alpha\hbar\omega)^{1/2}$ vs $\hbar\omega$ and its extrapolation to zero. Such results

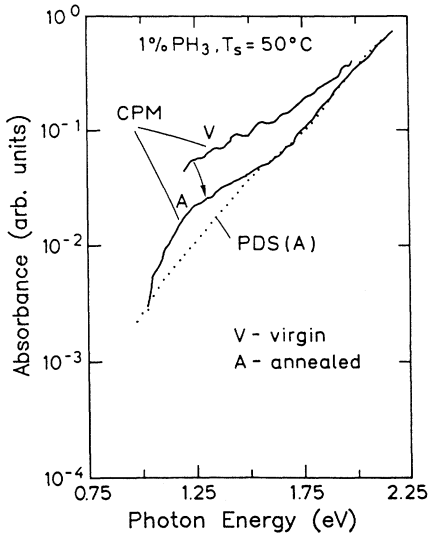

FIG. 3. Spectral dependence of the absorbance of 1% PH_3-doped *a*-Si:H:P, prepared at $T_s = 50$ °C, in the virgin (*V*) and 150 °C annealed (*A*) states deduced by CPM and PDS methods (see text). Absorbance $A = 1\text{-}R\text{-}T$, where R and T are reflectivity and transmission.

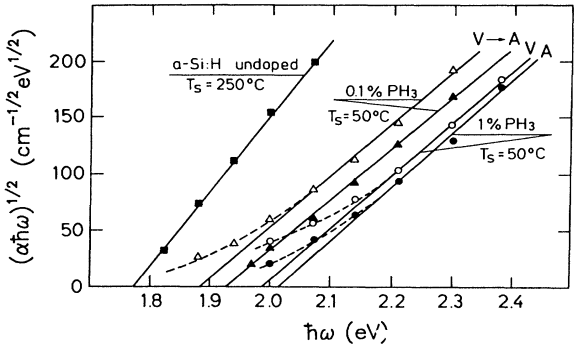

FIG. 4. Spectral dependences of $(\alpha\hbar\omega)^{1/2}$ of undoped a-Si:H prepared at $T_s=250\,^{\circ}\mathrm{C}$ and differently doped a-Si:H:P samples, prepared at 50 °C, in the virgin (V) and 240 °C annealed (A) states.

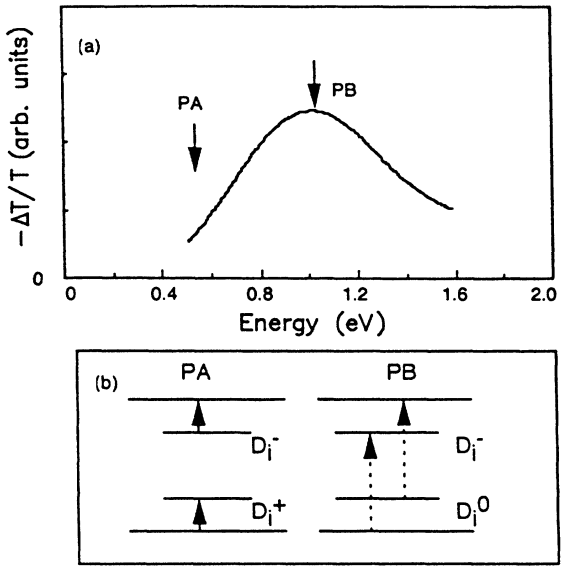

FIG. 5. (a) PM spectrum of undoped a-Si:H deposited at $T_s=250\,^{\circ}\mathrm{C}$, measured at 240 K. (b) Photoinduced absorption (PA) and bleaching (PB) in undoped a-Si:H. The transitions occur between a defect state and the conduction or valence bands.

are shown in Fig. 4 for undoped a-Si:H ($T_s=250\,^{\circ}\mathrm{C}$) and differently doped a-Si:H:P ($T_s=50\,^{\circ}\mathrm{C}$) virgin and annealed samples.

Two important features are apparent. First, the optical gap of P-doped low-T_s samples is 0.1–0.2 eV higher than the gap of device-quality (undoped or doped) a-Si:H. Moreover, E_g of low-T_s a-Si:H:P samples is a function of the P concentration; with increasing P concentration E_g increases. This indicates that P and H contents in low T_s samples are correlated as suggested in Ref. 21.

The second interesting fact is that the E_g of low-T_s a-Si:H:P samples changes with annealing. If the annealing induced H evolution, the optical gap would decrease. The observed opposite trend (an increase of E_g) shows that we can exclude the H evolution, and that therefore the annealing-induced changes in E_g are related to a substantial structural rearrangement.

C. Photomodulation spectra

We have obtained additional information about the states in the gap by applying the steady-state PM spectroscopy. This technique has the unique capability of determining defect energies in both the ground and excited states.[22]

In Figs. 5(a) and 6(a), we show the PM spectra of undoped a-Si:H and 0.1% PH_3-doped a-Si:H:P deposited at a substrate temperature $T_s=250\,^{\circ}\mathrm{C}$. In Fig. 7, on the other hand, we show the PM spectrum of an a-Si:H:P film with the same PH_3/SiH_4 doping ratio but deposited at a low substrate temperature ($T_s=50\,^{\circ}\mathrm{C}$), as well as the spectra of the same film annealed at 150° and 250 °C. In Fig. 8, we show similar data obtained on a 1% PH_3-doped film deposited at $T_s=50\,^{\circ}\mathrm{C}$.

It is meaningless to compare the absolute strengths of the steady-state PM spectra of various samples or differently treated samples because the strength of photoinduced optical absorption depends on the recombination time, which is not known. Therefore, only relative differences in the various parts of the spectra contain relevant information. We observe that the high-energy parts of the virgin and annealed samples shown in Figs. 7 and 8 have the same spectral shapes. It is therefore useful to scale the relative strength of both spectra so that the high-energy parts overlap.

From inspection of the PM spectra we see that the spectrum of the virgin sample in Figs. 7 and 8 resembles more closely that of undoped a-Si:H [Fig. 5(a)] than that

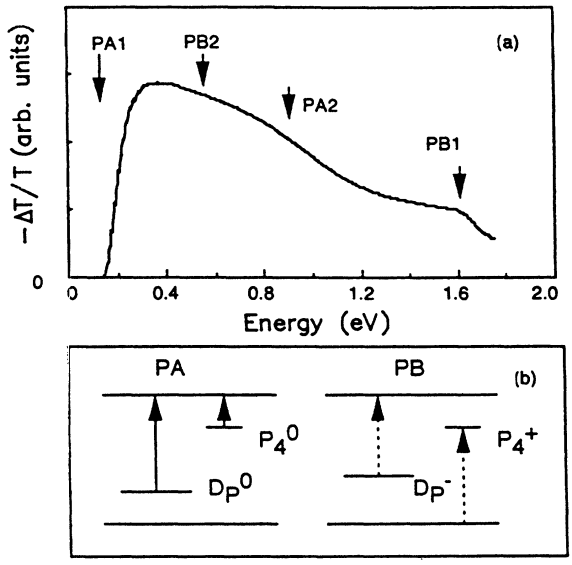

FIG. 6. (a) PM spectrum of 0.1% PH_3-doped a-Si:H:P deposited at 250 °C and measured at 80 K together with the illustration of PA and PB transitions (b).

of the doped a-Si:H:P shown in Fig. 6(a). As seen in Figs. 7 and 8, annealing adds considerable optical strength to the low-energy part of the virgin sample making it somewhat more similar to the a-Si:H:P spectrum in Fig. 6(a).

We will discuss a plausible origin of these rather striking differences and changes. Our interpretation is based on a model of the PM spectra of undoped and doped a-Si:H proposed by Vardeny *et al.*;[23] its somewhat modified form used in this paper is described in Ref. 24.

The room-temperature PM spectrum of undoped a-Si:H is ascribed to transitions associated with the "intrinsic" db state[18] D_i which, in the dark, is in the neutral state D_i^0. Photogenerated electrons and holes are trapped on D_i^0 and produce charged states D_i^- and D_i^+. As seen in Fig. 5(b), the changes in absorption are due to the removal of electron transitions $\mathrm{vb}\rightarrow D_i^-$ and $D_i^0\rightarrow\mathrm{cb}$ that exist in the dark [photoinduced bleaching (PB)] and to the transitions $\mathrm{vb}\rightarrow D_i^+$ and $D_i^-\rightarrow\mathrm{cb}$ [photoinduced absorption (PA)]. The onset of the PM spectrum is the PA transition (at 0.60 eV) followed by the PB transition (at 1.10 eV) as shown in Fig. 5(a). Since only one band is observed we assumed that all energy levels are symmetrical about midgap. Because $E(\mathrm{PA})+E(\mathrm{PB})=1.70\ \mathrm{eV}\cong E_g$ (optical gap $=1.75$ eV), the lattice relaxation of charged defects is very small[22] and we neglected it in Fig. 5(b). In a-Si:H:P deposited at 250 °C [Fig. 6(a)] the defects in the dark are D_P^- and P_4^+ which, after carrier trapping, change to D_P^0 and P_4^0. PA transitions are $P_4^0\rightarrow$cb (PA1) and $D_P^0\rightarrow$cb (PA2) while PB transitions are $\mathrm{vb}\rightarrow P_4^+$ (PB1) and $D_P^-\rightarrow$cb (PB2).[24]

In fact, the defect (db) and impurity energies are not sharp levels as shown in Figs. 5(b) and 6(b) but energy distributions. We have shown[24] that the spectra in Figs. 5(a) and 6(a) can be fitted using Gaussian distributions for the defect and an exponential conduction band tail that contains the P_4 states.[25] The pump light intensity in the PM experiments is sufficiently high to produce quasi-Fermi levels F_n and F_p which lie practically outside the db defect distributions so that the conversion from one charge state to another is complete.

In a-Si:H:P the quasi-Fermi level F_n lies in the cb tail. The states below F_n are P_4^0 and cb^- states. Because the tail has an exponential density of states (DOS), the product of the tail DOS function and the Fermi distribution function peaks close to F_n. This distribution moves only a little with the illumination intensity because it is located in a region of high DOS. Because we cannot distinguish in PM experiment the true Gaussian P_4 peak and peaked occupied cb tail states and assume that in our heavily doped a-Si:H:P the P_4 states prevail, we label both these (P_4 and cb tail) states jointly as P_4^0. The energy levels shown in Figs. 5(b) and 6(b) are the peaks of the Gaussian-defect energy distributions and the quasi-Fermi levels F_n separating P_4^0 and P_4^+.

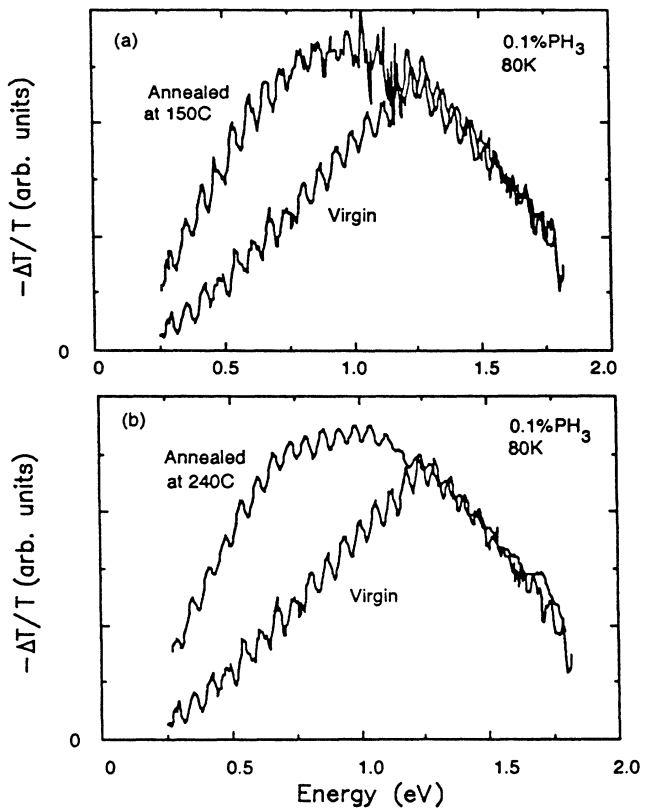

FIG. 7. PM spectrum of 0.1% PH_3-doped a-Si:H:P deposited at 50 °C in the virgin state and after annealing at 150 °C (a) and 240 °C (b).

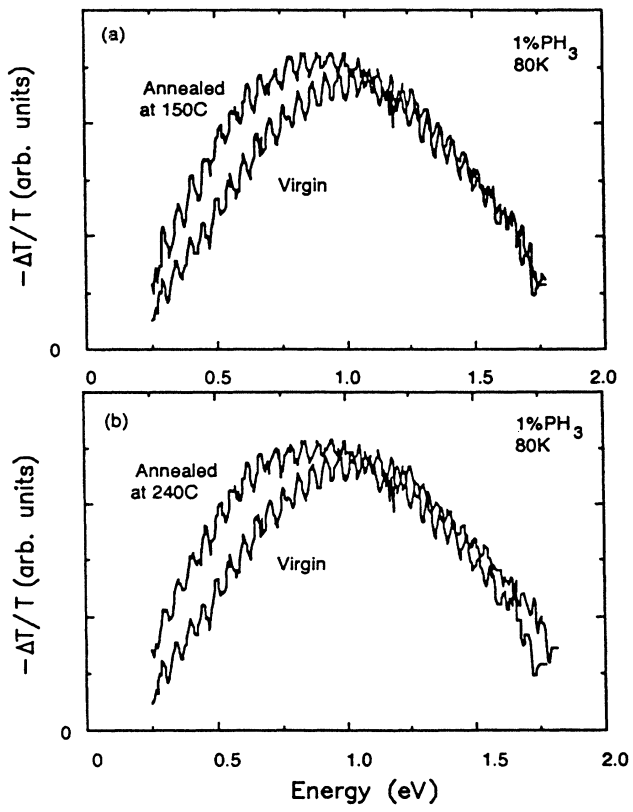

FIG. 8. PM spectrum of 1% PH_3-doped a-Si:H:P deposited at 50 °C in the virgin state and after annealing at 150 °C (a) and 240 °C (b).

The adjustable parameters of the distributions (positions of the peaks, the width of the Gaussians, F_n, and the relative strength of the various transitions) are obtained from optimizing a fit of the calculated spectrum with the measured spectrum. Since the k vector is not conserved, the absorption is calculated as proportional to the energy-conserving convolution of the distribution of the initial states with the distribution of the final states as described in Refs. 23, 24, and 26. The density of states in the band was assumed to be proportional to the square root of energy. The fitting parameters for undoped a-Si:H and 1% PH_3-doped a-Si:H:P deposited at 250 °C are shown in Table II.

We used this technique for the determination of the defect parameters and tail-distribution functions of a-Si:H:P deposited at $T_s = 50$ °C and of their changes produced by annealing. The results are summarized in Table III. The virgin spectrum can be fitted using transitions involving a defect with properties similar to the db in undoped a-Si:H. Transitions $D^0 \rightarrow$ cb and vb $\rightarrow D^+$ produce PA, transitions $D^0 \rightarrow$ cb and vb $\rightarrow D^-$ produce PB. We again assume a symmetrical energy distribution in the gap. There are, however, quantitative differences. The defect energies in low-T_s virgin samples are deeper in the gap compared to undoped a-Si:H. Also, the sum $E(\mathrm{PA}) + E(\mathrm{PB}) = 2.29$ eV is larger than E_g (1.88 eV), indicating lattice relaxation effects.[22]

As we mentioned above, the shape of the high-energy part of the PM spectrum of low T_s samples does not change with annealing. The difference spectrum shown in Fig. 9(a) is apparently due to states generated by annealing.

In a-Si:H:P deposited at 250 °C we described the low-energy part of the spectrum as a superposition of transitions $P_4^0 \rightarrow$ cb (PA) and $D_P^- \rightarrow$ cb (PB). With these transitions we fitted also the difference between the annealed spectrum and the virgin spectrum [shown in Fig. 9(a)], and obtained the distribution of the D^- and tail states shown in Fig. 9(b); the parameters for different cases are shown in Table III. The justification for this procedure is the similarity of the high-energy parts of the PM spectrum (Figs. 7 and 8), which suggests that the distribution of deeper states is not sensitive to annealing. However, their strength can be arbitrarily different in annealed and virgin samples; the PM spectrum only shows an increase of the gap states closer to the cb relative to the states deeper in the gap. The energies of D^- states in annealed low-T_s samples are about 0.1 eV deeper than D_P states in a-Si:H:P deposited at 250 °C ; the cb tail widths are somewhat larger (Tables II and III).

To conclude this section, PM spectra of virgin low-T_s a-Si:H:P samples can be described by a defect with properties similar to the D_i dangling bond in undoped a-Si:H. The observed changes produced by annealing are compatible with the assumption that annealing produces defects similar to P-related db in a-Si:H:P deposited at 250 °C. In both cases the similarity means the same combination of photoinduced absorption and bleaching properties. However, the energies of these defects are different from those in samples deposited at 250 °C (see Sec. IV).

TABLE II. Parameters obtained from the PM spectra of device-quality a-Si:H, and 1% PH_3-doped a-Si:H:P prepared at $T_s = 250$ °C. Energies of gap states are explained in the text. ΔE_D and E_0 are the widths of the Gaussian and exponential tail distributions. The position of the quasi-Fermi energy F_n was determined from fitting the spectra while the position of the Fermi level E_f was determined from the temperature dependence of electrical conductivity.

Energy (eV)	a-Si:H	a-Si:H:P
E_g	1.75	1.78
E_c-E (D_i^0)	1.10	
E_c-E (D_i^-)	0.60	
E_c-E (D_P^0)		1.21
E_c-E (D_P^-)		0.95
ΔE_D	0.21	0.23
E_c-E_f		0.19
E_c-F_n		0.15
E_0		0.07

D. Electron spin resonance

The experimental results presented so far are further complemented by ESR and LESR measurements performed at room temperature and at $T = 100$ K on samples that were deposited and annealed under the same

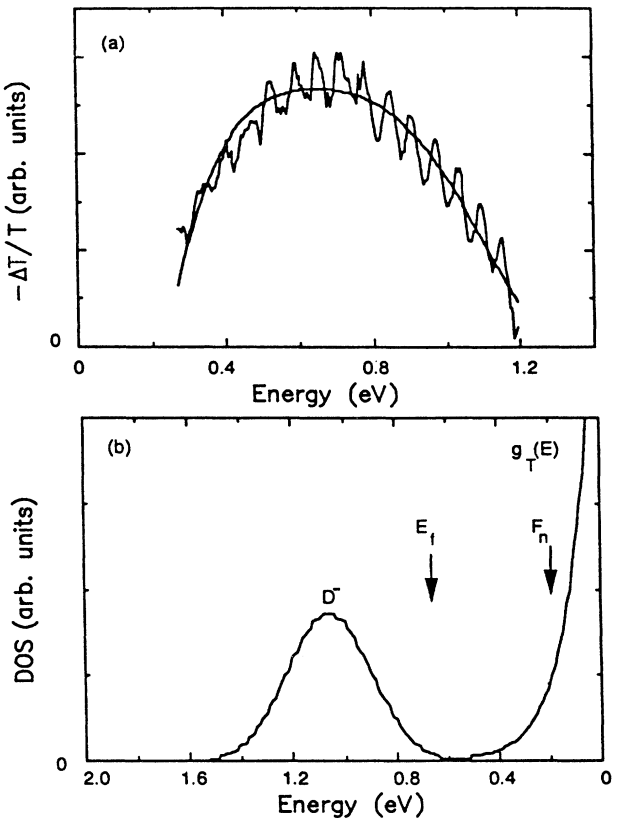

FIG. 9. (a) Difference of the PM spectra (annealed minus virgin) of low-T_s 0.1% PH_3-doped a-Si:H:P shown in Fig. 7. (b) Additional gap states produced by annealing and the positions of the Fermi (E_f) and quasi-Fermi (F_n) levels.

TABLE III. Parameters of low-T_s ($T_s = 50$ °C) a-Si:H:P. Same notations as in Table II. A and V denote annealing at 150° or 240 °C and Virgin, respectively.

	0.1% PH_3			1% PH_3		
Energy (eV)	V	$A150$	$A240$	V	$A150$	$A240$
E_g	1.88	1.90	1.93	1.99	2.00	2.02
E_c-E (D^-)	0.69	1.05	1.06	0.56	1.04	1.05
E_c-E (D^0)	1.6			1.45		
ΔE_D	0.32	0.22	0.22	0.27	0.31	0.32
E_c-E_f	0.69	0.66	0.65	0.49	0.40	0.40
E_c-F_n		0.21	0.21		0.21	0.18
E_0		0.10	0.10		0.11	0.11

conditions as those employed for the transport and optical experiments. For the case of the sample doped with 0.1% PH_3, ESR and LESR spectra ($T = 100$ K) are shown in Fig. 10. In the as-deposited, virgin state the sample exhibits a strong ESR signal due to neutral dangling bonds with a g value of $g = 2.0053$. The right-hand side of Fig. 10 shows the same spectrum over a broader magnetic-field scale. The ESR signal (dashed curve) clearly exhibits a resolved hyperfine structure due to the interaction of the dangling-bond electrons with ^{29}Si nuclei.[27] Upon illumination, the dangling-bond signal in the as-prepared material persists without any significant change. The broader magnetic-field scan, however, reveals an additional pair of hyperfine lines (solid curve) with a splitting of ≈ 250 G ascribed to a hyperfine interaction of un-ionized donors (P_4^0) with the ^{31}P nuclei.[4] Annealing at 150° and 250 °C causes a significant decrease of the dangling-bond-related ESR by almost two orders of magnitude, without a change in g value ($g = 2.0054$ after 150° and 250 °C anneal). In contrast to this strong decrease of the equilibrium ESR signal, the LESR signal at $g = 2.0054$ decreases only by a factor of ≈ 5. The annealing behavior of the dangling-bond ESR and LESR signals is also corroborated by the ^{29}Si hyperfine signal on the right-hand side of Fig. 10: The ^{29}Si hyperfine structure disappears almost completely in the ESR response of the annealed samples, but it can be partly recovered under illumination (LESR). In contrast, the ^{31}P hyperfine doublet appears more prominently in the equilibrium ESR spectrum with increasing annealing temperature. At the same time, the relative increase of this signal in LESR is reduced from a factor of approximately 10 in the virgin state to a change by less than 40% after annealing at 250 °C. Quantitative results for spin densities associated with the different defect states deduced from the spectra in Fig. 10 are summarized in the upper part of Table IV.

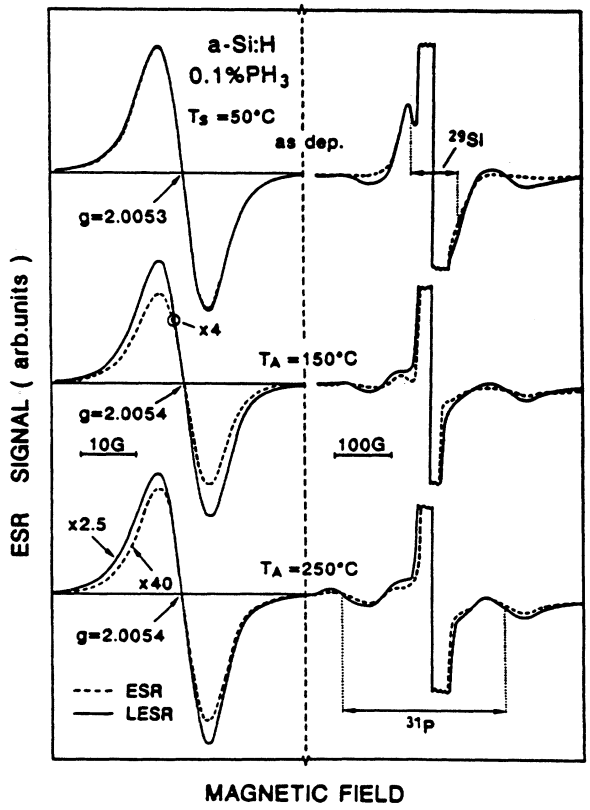

FIG. 10. Electron-spin-resonance spectra of n-type a-Si:H ($T_s = 50$ °C, 0.1 vol.% PH_3) in the as-deposited state and after annealing at 150 °C and 250 °C, respectively. Dashed curves represent equilibrium ESR spectra, solid curves show the LESR response at $T = 100$ K. Note the different scaling factors for the spectra of annealed samples. The left-hand side of the figure shows the central resonance around $g \approx 2.0054$ (dangling-bond signal), whereas the right-hand side was obtained with an extended magnetic-field scale for the detection of ^{29}Si and ^{31}P hyperfine structure.

If the doping level of the material deposited at low T_s is increased to 1%, quite different ESR and LESR responses are observed. In the as-prepared state, ESR shows a much smaller dangling-bond-related ESR signal and, at the same time, a much larger ^{31}P hyperfine contribution (dashed curves in the lower part of Fig. 11). When the sample is illuminated at low temperatures, the db signal increases by about a factor of 4, while the line position remains at the relatively low g value of 2.0051. The ^{31}P hyperfine doublet increases by a factor of 2. The main effect of annealing is an order-of-magnitude decrease of the equilibrium dangling-bond ESR signal, whereas all other ESR and LESR spin densities exhibit no significant variation (middle part of Table IV).

In order to provide a better visualization of the annealing-induced changes in the LESR and ESR

TABLE IV. ESR and LESR spin densities measured at 100 K (T_s and T_A are substrate and annealing temperatures, respectively, db denotes dangling bonds, cb denotes conduction-band tail electrons, hf denotes ^{31}P hyperfine states). See text.

PH_3/SiH_4	T_s (°C)	T_A (°C)	ESR N_s(db)	LESR (cm^{-3})	ESR N_s(cb)	LESR (cm^{-3})	ESR N_s(hf)	LESR (cm^{-3})
0.1%	50		1.8×10^{18}	1.8×10^{18}				1.4×10^{17}
		150	3.2×10^{17}	4.3×10^{17}			6×10^{16}	1.5×10^{17}
		250	3.5×10^{16}	6.5×10^{17}			9×10^{16}	1.3×10^{17}
1%	50		1×10^{17}	4.4×10^{17}			1.5×10^{17}	3.0×10^{17}
		150	$\approx1\times10^{16}$	4.5×10^{17}	$\approx2\times10^{16}$		9×10^{16}	3.0×10^{17}
		250	$\approx1\times10^{16}$	4.4×10^{17}	$\approx2\times10^{16}$		1.8×10^{17}	4.3×10^{17}
1%	230				4×10^{16}	7×10^{16}	1.3×10^{17}	1.4×10^{17}

responses of low-temperature-deposited *a*-Si:H, we have summarized the spin-resonance results again in Fig. 12 for the two PH_3-doping levels employed in the present study.

For the purpose of comparison we have included in Table IV (lower part) as well as in Fig. 11 the ESR and LESR data for device-quality *a*-Si:H deposited at $T_s=230$ °C with a doping level of 1% PH_3. Device-quality material shows almost no changes of the ^{31}P hyperfine doublet upon low-temperature illumination, and only a small increase of the central resonance line near $g=2$. Note also that the g value of this central line is at $g=2.0044$, a value usually ascribed to single electrons trapped in localized conduction-band tail states.[28] It has also been suggested in the literature[29] that the line at $g=2.0044$ is due to dangling-bond-like defects in different microscopic environments. However, for the present study, details of the intrinsic spin defects in *a*-Si:H and their corresponding g values are not of direct importance. It is only required that the defect levels associated with the $g=2.0044$ spin-resonance line have an energy position close to the conduction-band tail, as opposed to the deep midgap levels with a g value of 2.0055. Therefore, in this paper we use the assignment of the $g=2.0044$ resonance to electrons trapped in conduction-band tail states without further discussion.

There are two important conclusions that can be drawn from our spin-resonance results concerning the various electronic levels in *n*-type *a*-Si:H deposited at low

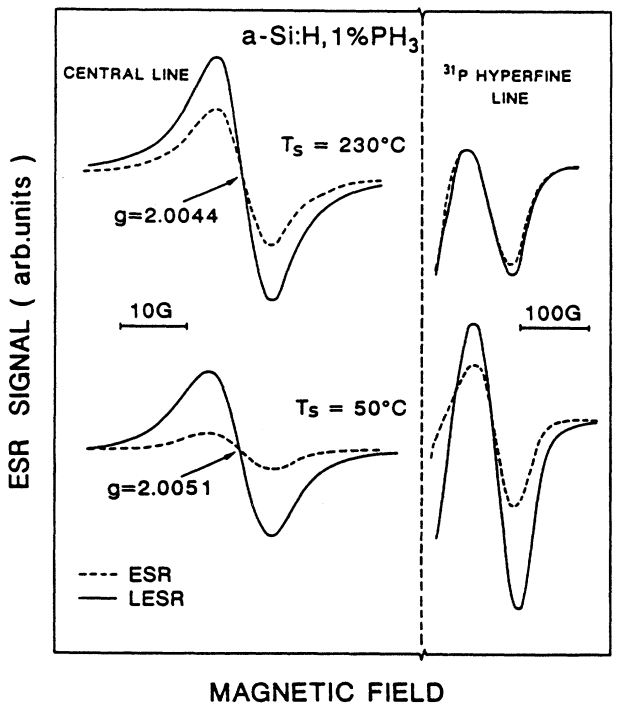

FIG. 11. Comparison of the ESR and LESR responses in *n*-type *a*-Si:H doped with 1 vol.% PH_3 and deposited at a substrate temperature of 50 °C (lower part) and 230 °C (upper part). The measurement temperature was 100 K for all spectra. The central line in the vicinity of $g\approx2$ is shown on the left-hand side, the high-field resonance of the ^{31}P hyperfine doublet on the right-hand side of the figure.

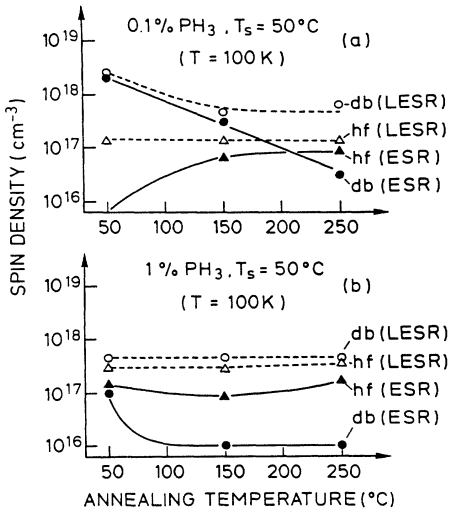

FIG. 12. Dependence of the spin densities ($T=100$ K) in *n*-type *a*-Si:H prepared at low substrate temperatures, $T_s=50$ °C, on the annealing temperature: (a) 0.1% PH_3, (b) 1% PH_3. ESR data are represented by solid symbols and curves, LESR data by open symbols and dashed curves, respectively. db and hf refer to dangling bonds and ^{31}P hyperfine resonances.

substrate temperatures: (i) The equilibrium ESR spin densities are very unreliable in determining the relative densities of defect states and donor levels, and (ii) low-T_s material after annealing at 250 °C is still different from material deposited at 250 °C. This latter observation is qualitatively in agreement with the conclusions drawn from the transport and photomodulation experiments described in the previous sections.

The strong discrepancy between ESR and LESR spin densities in low-T_s material compared to the small light-induced ESR changes in device-quality n-type a-Si:H prepared at $T_s = 230$ °C can only be explained if we involve pronounced potential fluctuations in low-T_s samples. This is shown schematically in Fig. 13. In device-quality n-type a-Si:H, P_4 donor atoms and compensating dangling bonds are homogeneously distributed throughout the sample with $[P_4^+] \approx [D^-]$. There are relatively small potential fluctuations due to the presence of dopants, in particular if P_4^+ states and D^- states are spatially correlated as suggested by one of the present authors.[18] The dark ESR shows no dangling-bond signal since the Fermi-level E_f in the entire sample lies within the conduction-band tail at $E_f \approx E_c - 0.2$ eV. The LESR response is also small ($\approx 30\%$ of the equilibrium spin density) because of the short lifetime of photoexcited carriers.

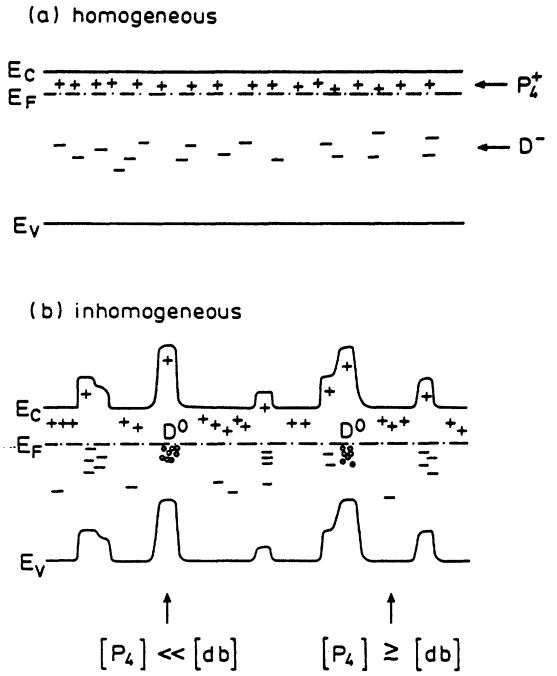

FIG. 13. Schematic diagram showing the differences between homogeneous n-type a-Si:H obtained through deposition at 230 °C (a), and in homogeneous material formed during low-temperature deposition (b). E_C, E_F, and E_V indicate the local conduction-band mobility edge, the Fermi level in equilibrium, and the valence-band mobility edge, respectively. D^0 and D^- denote neutral and negatively charged dangling-bond defects, P_4^+ stands for ionized phosphorus donor levels. See text for further discussion.

In contrast to this "normal" behavior, the lower part of Fig. 13 illustrates how the large potential fluctuations due to an inhomogeneous distribution of dangling bond defects and/or dopant atoms can cause a completely different situation in a-Si:H deposited at low substrate temperatures. Such an inhomogeneous distribution can occur because low-T_s material already possesses a very high density of dangling-bond defects ($\approx 10^{18}$ cm^{-3}) that are related not to doping but to incomplete Si-bond termination during deposition. The main difference that is important here is that the dangling bonds in n-type samples deposited at low substrate temperatures no longer need to be correlated (spatially as well as in density) with the dopant atoms. Therefore, we can have regions in the samples with dangling-bond densities largely in excess of the density of active dopants, but also other parts where the dopant density is equal to or even larger than the dangling-bond density. One result of this is that effectively doped regions alternate with essentially intrinsic regions, as indicated in Fig. 13(b). These alternations cause additional potential fluctuations and are also responsible for the different optical and transport properties of low-T_s n-type a-Si:H compared to material deposited at 230 °C. In the case of equilibrium dark ESR, the situation shown in Fig. 13(b) also explains why deep dangling-bond defects and shallow P_4^0 states can be observed simultaneously in one sample. This would be impossible (and is not observed) in the homogeneous situation of Fig. 13(a).

However, there are also more subtle effects in low-T_s n-type a-Si:H that are revealed by the LESR data summarized in Fig. 12 and Table IV. One important observation is that the doping efficiency in low-T_s material is significantly higher than in device-quality material. This is due to the fact that the high dangling-bond density in defective regions pins the Fermi level near midgap and increases the formation probability of active P_4 states. In the doping model suggested by Street,[2] the increased doping efficiency in defective a-Si:H is explained via the compensation of excess donor charge by the much larger deep-defect density. If the background defect density is low, as in device-quality material, dopant compensation requires the formation of excess defect states. This is energetically unfavorable and decreases the doping efficiency. If, as proposed in the context of Fig. 13, compensating defects in low-T_s a-Si:H are essentially spatially separated from the active donor sites, the charge compensation responsible for the increased doping efficiency can be easily reversed by illumination at low temperatures: photoexcited electrons are predominantly trapped by P_4^+ states in low-defect regions, whereas photoexcited holes are mainly captured by D^- defects in high-defect-density regions. The result is a strong LESR response similar to the one observed[4] in compensated a-Si:H. The observed LESR spin densities due to P_4^0 and D^0 states then provide a lower limit for the overall density of active donors and compensating defects in a given sample. A quantitative test for the validity of this interpretation of the LESR results is that in cases where the deep-defect density is not dominated by doping-induced states, the observed LESR spin density due to dangling bonds (i.e.

background and doping induced) should be equal to or larger than the spin density due to active dopants. This is indeed observed (see open circles and open triangles in Fig. 12).

A further observation is that the lower limit for the total dangling-bond defect density in the low-T_s samples studied here by LESR is fairly insensitive to annealing (up to 250 °C) and to changes in the doping level. The maximum variation observed is approximately a factor of 4. On the other hand, experimental quantities that depend on the averaged difference between shallow- and deep-defect densities, such as the equilibrium ESR spin densities, the dark conductivity, or the Fermi-level position, show much larger variations with annealing temperature and doping level. It is, therefore, probably misleading[7] to base an analysis of the densities and energy positions of dopants and defects on such quantities, in particular if changes in deposition conditions or impurity (dopants) incorporation are involved.

IV. DISCUSSION AND CONCLUSIONS

There is a basic controversy concerning the microscopic origin of the P-related hf signal (shallow P_4^0 versus deep P_4^0 or "weak" P_4^0). The recent papers[6–8] used the following implicit assumptions. First, the P_4^0 center in device-quality ($T_s = 250$ °C) and low-T_s samples is identical. Second, the electron mobility edge (transport path—E_c) is fixed and only the Fermi level changes, and third, the samples are homogeneous. We will illustrate that the controversy is related to the fact that none of the above assumptions is fully true.

From Table III and Fig. 14 (see below) it is seen that the P_4^0 state in low-T_s a-Si:H:P appears to be about 0.1 eV deeper (relative to E_c) than in the device-quality a-Si:H:P.

Does it mean that P_4^0 in low-T_s samples is different? In principle, a deeper P_4^0 state could be related with a H atom sitting near the P atom.[30] High H concentration, which is moreover correlated with the P concentration (see Sec. III B and Ref. 21), is typical for low-T_s samples.[9]

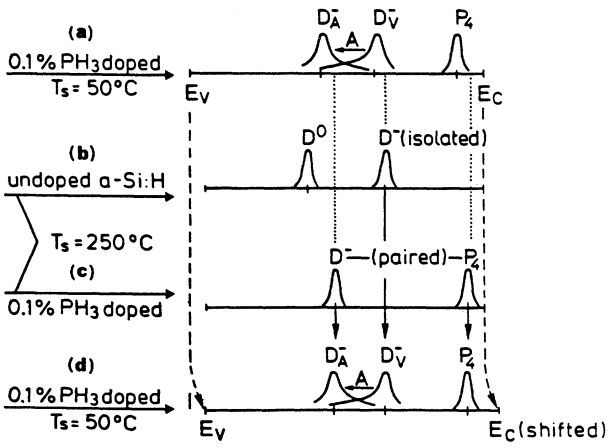

FIG. 14. Schematic illustration of the energy positions of the dominant defects obtained by the deconvolution of PM spectra for different a-Si:H samples in the virgin (V) and annealed (A) states.[34] See text.

Although we believe that the shift of E_c is an alternative and more probable origin of the deeper P_4^0 states in low-T_s samples (see below), the influence of H cannot be fully excluded.

What can we say about E_c when the substrate temperature decreases from 250° to 50 °C? The behavior of the activation energy (E_a) and the prefactor σ_0, which is in conflict with the Meyer-Neldel rule (see Sec. III A and Table I) is a strong indication that the macroscopic transport path (E_c) is shifted. Recently, very general explanation of the Meyer-Neldel rule, based on the thermodynamical arguments and not on the density of states,[16] has been presented by Yelon, Movaghar, and Branz.[31] Within their model the above-mentioned anti-Meyer-Neldel behavior, observed by us, is the sign of the change of the activation process leading to the macroscopic transport. This represents from another point of view what we call "the shift of the transport path."

The larger optical gap of low-T_s samples indicates that an upward shift of E_c is possible. Let us have a look at the PM spectra of low-T_s samples and their changes with annealing. The data from Tables II and III are illustrated graphically in Fig. 14. For the case of 0.1% PH_3-doped low-T_s a-Si:H:P sample, the shapes of the PM spectra and their detailed analyses have shown (see Sec. III C) that in the virgin state the dominant deep defect is similar to the intrinsic ("isolated")[18] dangling bond in undoped device-quality a-Si:H [see Figs. 14(a) and 14(b)]. As is clearly seen from the CPM spectra in Fig. 3, annealing changes only slightly the total concentration of deep defects, however, the change of the PM spectral shape indicates that the energy positions of the dominant deep defects change strongly (see Figs. 7 and 8). In analogy with undoped low-T_s a-Si:H (Ref. 19), the concentration of intrinsic db decreases by annealing and at the same time the deeper defect (D_A^-) becomes dominant [see Fig. 14(a)]. The position of this deeper defect [D_A^- in Fig. 14(a)] is similar to the P-related db in P-doped device-quality a-Si:H [see Figs. 6 and 14(c)].

When we compare the positions of the dominant states in undoped and 0.1% PH_3-doped $T_s = 250$ °C samples and in the 0.1% PH_3-doped $T_s = 50$ °C sample, one notices that, assuming E_c is fixed [Figs. 14(a)–14(c)], all levels (isolated db, P-related db, and P_4) are about 0.1 eV deeper in the $T_s = 50$ °C sample. If we shift E_c up by 0.1 eV [Fig. 14(d)] all levels in the different samples precisely coincide. This is an indication that although a downward shift of the valence-band edge (E_v) is usually assumed[9] with increasing H content (decreasing T_s), there is also an upward shift of E_c by about 0.1 eV.

We can summarize the above discussion concerning the position of E_c as follows. On the basis of the transport data, it is clear that E_c shifts when we change T_s from 250 °C to 50 °C. Increasing optical gap and the above PM results indicate at least a 0.1 eV upward shift of E_c.

Up to now we have assumed that the low-T_s samples are spatially homogeneous. When we admit that there are potential fluctuations in these samples then the real upward shift of the "transport path" can be 0.2–0.3 eV,

that is, larger than $\Delta E_c = 0.1$ eV estimated above from the optical data.

Such shift of the transport path ($\Delta E_c \approx 0.2-0.3$ eV) in low-T_s samples would explain the basic disagreement—the fact that the activation energy of the electrical conductivity is $E_a \approx 0.59$ eV (Ref. 7) and the P_4 state is still occupied.

There are two strong arguments supporting the existence of the potential fluctuations in low-T_s samples.

First is the direct estimate of the magnitude of the potential fluctuations from the combined thermopower (S) and electrical conductivity (σ) measurements[32] from which one can deduce the parameter $Q = \ln\sigma + eS/k$. The activation energy E_Q of this parameter is proportional to the amplitude of potential fluctuations.

The results of these measurements[33] for the 1% PH_3-doped, $T_s = 50$ °C sample gave an activation energy $E_Q \approx 0.3$ eV in the virgin state which, after annealing, decreased to $E_Q \approx 0.22$ eV. These results confirm the existence of quite strong potential fluctuations in low-T_s samples,[32] which decrease but do not disappear with annealing. E_Q of comparably doped high-T_s samples is $E_Q \approx 0.15$ eV and for device-quality undoped a-Si:H $E_Q \approx 0.05$ eV.

In device-quality a-Si:H:P the E_f is close to the cb edge ($E_a = 0.19$ eV) and so the db signal is not observable, and light-induced ESR is almost identical to dark ESR for the hf line and a small increase is observed for cb tail electrons (see Table IV).

Contrary to this, for the low-T_s sample in both the virgin and annealed states a strong increase of the hf signal with illumination (ESR→LESR) is observed; an even larger relative increase is seen for the db signal (Table IV).

The natural explanation for this metastable charge transfer ($D^- + P_4^+ \leftrightarrow D^0 + P_4^0$) is that the photoexcited carriers are spatially separated due to potential fluctuations. A relatively long lifetime of the LESR signal is a consequence of this spatial carrier separation. These ESR results represent the second argument for the existence of the potential fluctuations.

The potential fluctuations imply that there are regions where E_f is close to the E_c and regions where E_f is close to the midgap. This naturally explains the surprising coexistence of the db and hf signals in low-T_s samples. We believe that a heterogeneous sample, in which regions with cb electronlike and db-like dominant defects coexist, has a stronger tendency toward sharp g-value conversion[8] than a homogeneous one.

We can summarize the results as follows.

(1) Although we cannot exclude that the P_4 level is broader than was originally assumed, mainly the temperature dependence[4] and the doping-level dependence of the dangling bond and P hyperfine signal leads us to the conclusion that P hyperfine-related states must be shallow.

(2) The experiment facts, mainly the LESR and transport data, support our conclusion that seemingly controversial results, namely the appearance of hyperfine ESR signal in P-doped low-T_s samples with $E_a \approx 0.5$ eV can be explained by the existence of potential fluctuations.

(3) We have documented that not only E_f but also E_c can move when substrate temperature changes, so that the real problem is the finding of a reliable energy reference point.

(4) We also note that a-Si:H:P (contrary to undoped a-Si:H) deposited at $T_s = 50$ °C even after annealing at 250 °C is different from a-Si:H:P deposited at $T_s = 250$ °C.

ACKNOWLEDGMENTS

The authors would like to thank W. Beyer for some of the transport measurements. The financial support of ČSAV Grant No.11063 (IP-Prague), National Science Foundation Grant No. DMR 9014977 (Brown University-Providence), and BMFT Contract No. 0328962A (MPI-Stuttgart) is acknowledged.

[1] W. E. Spear and P. G. LeComber, Philos. Mag. **33**, 935 (1976).
[2] R. A. Street, Phys. Rev. Lett. **49**, 1187 (1982).
[3] H. Dersch, I. Stuke, and J. Beichler, Phys. Status Solidi B **105**, 265 (1981).
[4] M. Stutzmann and J. Stuke, J. Non-Cryst. Solids **66**, 145 (1984); M. Stutzmann, D. K. Biegelsen, and R. A. Street, Phys. Rev. B **35**, 5666 (1987).
[5] I. Hirabayashi, M. Morigaki, S. Yamasaki, and K. Tanaka, in *Optical Effects in Amorphous Semiconductors,* Proceedings of the International Topical Conference on Optical Effects in Amorphous Semiconductors, edited by P. C. Taylor and S. G. Bishop, AIP Conf. Proc. No. 120 (AIP, New York, 1984), p. 8.
[6] N. Ishii, M. Kumeda, and T. Shimizu, Solid State Commun. **53**, 543 (1985).
[7] S. Yamasaki, S. Kuroda, H. Okushi, and K. Tanaka, J. Non-Cryst. Solids **77/88**, 339 (1985).
[8] S. Schütte, F. Finger, and W. Fuhs, J. Non-Cryst. Solids **114**, 411 (1989).
[9] W. Grevendonk, M. Verluyten, J. Dauwen, G. J. Andriaenssens, and J. Bezemer, Philos. Mag. B **61**, 393 (1990).
[10] J. Kočka, M. Vaněček, and A. Tříska, in *Amorphous Silicon and Related Materials,* edited by H. Fritzsche (World Scientific, Singapore, 1989), p. 297.
[11] H. Curtins and M. Favre (Ref. 10), p. 329.
[12] Z. Vardeny, T. X. Zhou, and J. Tauc (Ref. 10), p. 513; see also H. T. Grahn, C. Thomsen, and J. Tauc, Opt. Commun. **58**, 226 (1986).
[13] J. Stuke, J. Non-Cryst. Solids **97/98**, 1 (1987).
[14] J. Kakalios and R. A. Street, J. Non-Cryst. Solids **97/98**, 767 (1987).
[15] W. Meyer and H. Neldel, Z. Tech. Phys. **18**, 588 (1937).
[16] W. Beyer and H. Overhof, in *Semiconductors and Semimetals,* edited by J. I. Pankove (Academic, New York, 1984), Vol. 21, Pt. C, p. 257.
[17] M. Vaněček, J. Kočka, P. Demo, E. Šípek, and A. Tříska, J. Non-Cryst. Solids **90**, 183 (1987).
[18] J. Kočka, J. Non-Cryst. Solids **90**, 91 (1987).
[19] G. N. Parsons, C. Wang, M. J. Williams, and G. Lucovsky, Appl. Phys. Lett. **56**, 1895 (1990).

[20]J. Tauc, A. Abrahám, L. Pajasová, R. Grigorovici, and A. Vancu, *Proceedings of the International Conference on the Physics of Non-Crystalline Solids, Delft, 1964* (North-Holland, Amsterdam, 1964), p. 606.

[21]S. Hayashi, K. Hayamizu, S. Yamasaki, A. Matsuda, and K. Tanaka, Phys. Rev. B **38**, 31 (1989).

[22]Z. Vardeny and J. Tauc, Phys. Rev. Lett. **54**, 1844 (1985); Y. Bar-Yam, J. D. Joannopoulos, and D. Adler, Phys. Rev. Lett. **55**, 138 (1985).

[23]Z. Vardeny, T. X. Zhou, H. A. Stoddart, and J. Tauc, Solid State Commun. **65**, 1049 (1988).

[24]L. Chen, J. Tauc, J. Kočka, and J. Stuchlík, Phys. Rev. B **46**, 2050 (1992); J. Kočka, J. Stuchlík, M. Stutzmann, L. Chen, and J. Tauc, J. Non-Cryst. Solids **137/138**, 379 (1991).

[25]In Ref. 23 the distribution of P_4 states was assumed to be Gaussian. The fitting is not very sensitive to the exact form of the band-tail-state energy distribution as long as in the range around F_n it is a function that steeply decreases into the gap. In this case the electron distribution sharply peaks at F_n. For a Gaussian distribution of band-tail states one may expect that at the pump intensity used in our measurements F_n should be close to the peak of the Gaussian distribution.

[26]H. A. Stoddart, Z. Vardeny, and J. Tauc, Phys. Rev. B **38**, 1362 (1988).

[27]M. Stutzmann, D. K. Biegelsen, Phys. Rev. B **40**, 9834 (1989).

[28]M. Stutzmann, Phys. Rev. B **35**, 9735 (1987).

[29]S. Tamasaki, H. Okushi, S. Matsuda, and K. Tanaka, Phys. Rev. Lett. **65**, 756 (1990), and references therein.

[30]For the role of H, see papers in *Hydrogen in Semiconductors: Bulk and Surface Properties, Proceedings of the Sixth Trieste IUPAP-ICTP Semiconductor Symposium, 1990,* edited by M. Stutzmann and J. Chevallier (North-Holland, Amsterdam, 1991).

[31]A. Yelon, B. Movaghar, and H. M. Branz, Phys. Rev. B **46**, 12 244 (1992).

[32]W. Beyer, H. Overhof (Ref. 16), p. 257.

[33]W. Beyer (private communication).

[34]J. Kočka, J. Stuchlík, M. Stutzmann, L. Chen, and J. Tauc, J. Non-Cryst. Solids **137/138**, 379 (1991).